

## Generation of OAM Waves and Analysis of Mode Purity for 5G Sub-6 GHz Applications

Shehab Khan Noor<sup>1</sup>, Arif Mawardi Ismail<sup>1</sup>, Mohd Najib Mohd Yasin<sup>1,\*</sup>, Mohamed Nasrun Osman<sup>1</sup>, Nurulazlina Ramli<sup>2</sup>, Ali H. Rambe<sup>3</sup> and J. Iqbal<sup>4,5</sup>

<sup>1</sup>Advanced Communication Engineering (ACE), Centre of Excellence, Faculty of Electronic Engineering Technology, Universiti Malaysia Perlis, Kangar, Perlis, Malaysia

<sup>2</sup>Centre for Advanced Electrical & Electronic System (CAEES) Faculty of Engineering, Built Environment and Information Technology, SEGi University Petaling Jaya, Selangor, Malaysia

<sup>3</sup>Department of Electrical Engineering, Universitas Sumatera Utara, Medan, 20155, Indonesia

<sup>4</sup>School of Electrical and Electronic Engineering, Engineering Campus, Universiti Sains Malaysia, Nibong Tebal, 14300, Penang, Malaysia

<sup>5</sup>Faculty of Engineering & Technology, Gomal University, 29050 kpk, Pakistan

\*Corresponding Author: Mohd Najib Mohd Yasin. Email: najibyasin@unimap.edu.my

Received: 11 April 2022; Accepted: 29 June 2022

**Abstract:** This article presents the generation of Orbital Angular Momentum (OAM) vortex waves with mode 1 using Uniform Circular Array (UCA) antenna. Two different designs, namely, UCA-1 (4-element array antenna) and UCA-2 (8-element array antenna), were designed and fabricated using FR-4 substrate to generate OAM mode 1 at 3.5 GHz (5G mid-band). The proposed antenna arrays comprised rectangular microstrip patch elements with inset fed technique. The elements were excited by a carefully designed feeding phase shift network to provide similar output energy at output ports with desired phase shift value. The generated OAM waves were confirmed by measuring the null in the bore sight of their 2D radiation patterns, simulated phase distribution and intensity distribution. The measurement results agree well with the simulation results. Moreover, a detailed mode purity analysis of the generated OAM waves was carried out considering different factors. The investigation found that the greater the number of elements, the higher the purity of the generated OAM wave. Compared with other previous works, the proposed antenna design of this paper is very simple to design and fabricate. In addition, the proposed antennas are compact in design even at lower frequency band with very wide bandwidth to meet the requirements of 5G mid-band applications.

**Keywords:** Orbital angular momentum; vortex waves; fifth generation wireless communications; uniform circular array antenna; patch antenna

### 1 Introduction

Every year, the number of people subscribing to mobile broadband systems continues to increase substantially. People constantly prefer faster Internet connections, more appealing mobile phones,



This work is licensed under a Creative Commons Attribution 4.0 International License, which permits unrestricted use, distribution, and reproduction in any medium, provided the original work is properly cited.

and rapid connectivity with others to share data [1]. As a result, wireless mobile devices and services have grown massively. Furthermore, mobile telecommunication providers are encountering an ever-increasing demand from new wireless applications for higher data rates, broader network capacity, high spectral efficiency, higher energy efficiency, and greater flexibility. Smartphone traffic is anticipated to expand tenfold between 2017 and 2022, while overall mobile traffic will increase eightfold [2]. With the limited capability of earlier wireless generation technologies, managing this massive quantity of mobile data traffic is difficult. With present technologies, 4G networks have almost reached the theoretical data rate limit and are inadequate to handle the above-stated difficulties [3]. To solve the above issue, researchers have decided to move to a higher unused frequency spectrum to replace 4G with 5G. Compared to the present 4G networks, 5G networks will enable 10- to 100-times faster data rates with up to 10-times lower latencies. This can be achieved through more efficient radio technology (spectral efficiency) and more spectrum bandwidth (spectral capacity). The latest fifth-generation (5G) system is expected to be 100 times faster than the previous 4G system with new services such as smart homes, smart cars, the Internet of Things (IoT), and so on. As an outcome, 5G technology has risen to the top of the 2020 generation's demand list. The next generation of technology would enable high data rates, lower latency, additional capacity, and excellent quality of service. It is worth noting that 5G technology will open up new methods to overcome existing development limitations.

One possible way to utilize 5G wireless communication is by using Orbital Angular Momentum (OAM) vortex waves instead of conventional plane waves. The primary reason to use OAM waves instead of conventional plane waves is that OAM wave has the potential to allow infinite channels for wireless communication at Radio-Frequency (RF), giving it a new degree of freedom [4,5]. OAM wave has a large number of available topological charges, which are also known as OAM-modes. Different OAM-modes are orthogonal to each other, which would allow them to be multiplexed together to increase channel capacity [6]. Since an OAM wave has the potential to carry different modes, a new way can increase the spectrum efficiency. Accordingly, the OAM wave can be used for the upcoming 5G wireless communication system where higher data rates, spectrum efficiency, and security are in user demand. It was realized that the Orbital Angular Momentum (OAM) property (helical phased beams) of EM waves gives a rotational degree of freedom in the EM field by a phase factor  $\exp(il\phi)$ , where  $i$  the imaginary number,  $l$  is the topological charge and  $\phi$  is the azimuthal angle [7,8]. As there is a phase rotation factor, the wavefront has a spiral shape instead of the planar shape, as demonstrated in Fig. 1. This phase rotation factor is not present in plane waves, and this is what separates plane waves and OAM waves.

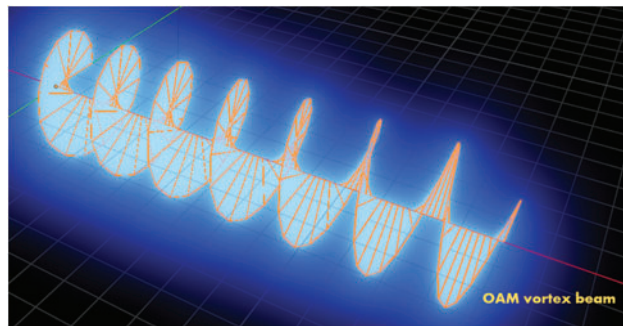


**Figure 1:** OAM vortex wave with mode 1 propagation

In literature, various methods are proposed to generate OAM waves [9]. However, the uniform circular array is considered the matured approach to generating OAM waves due to its great adaptability,

capacity to generate multiple OAM modes, compactness, and low cost [10]. In [11], the authors have designed a circular phased antenna array to generate OAM mode 1, where four identical rectangular patches were used to operate at 2.5 GHz. Although the measurement results have proved that they have generated OAM waves based on the spiral wavefront, the purity of the generated OAM mode is not discussed. Ke bi et al. [12] designed a Global Positioning System (GPS) ceramic array antenna to generate a negative mode ( $-1$ ) at 1.550 GHz. In this design, six antenna elements were placed on a ceramic substrate with a thickness of 4 mm and permittivity of 21.4; however, the obtained gain value is not disclosed in the paper. Moving to a frequency of 73.5 GHz, the authors in [13] have designed two dipole antenna arrays, one with eight elements and the other with 12 elements, to generate OAM mode  $+1$  and  $+3$ , respectively. The substrate used in both designs was FR4 with a thickness of 0.127 mm and permittivity of 3.75. The simulated gain achieved by the 8-element dipole array for mode 1 was 3.81 dB, while the gain achieved by the 12-element dipole array for mode 3 was 2.53 dB. However, the measured values are not disclosed. From the literature, it can be seen that the majority of the authors ignored the OAM mode purity information. Previous works have only focused on generating OAM waves with a helical wavefront. So far, it has been understood that generating OAM beams with a spiral phase distribution is essential to make sure the modes are orthogonal to one another; however, very little research has been carried out on the purity of generated OAM modes. Only having spiral phase distribution is insufficient to utilize the intrinsic characteristics of OAM beams. Factors such as the number of elements, observation plane size, and receiver size must be considered to generate OAM modes with high purity. Regarding the practical potential of the OAM antenna, it is essential to ensure the generate mode is high in purity while maintaining a helical wavefront for the modes to be orthogonal to one another for efficient data transmission.

In this work, two uniform circular antenna arrays (UCA) at 5G mid-band (3.5 GHz) were designed, fabricated, measured, and compared in terms of bandwidth, OAM mode purity, and helical wavefront. The first design (UCA-1) comprises four identical radiating elements (patches), while the second design (UCA-2) comprises eight identical elements (patches). The antenna elements are rectangular microstrip patches with an inset feed technique. A comprehensive analysis of mode purity for different numbers of elements, observation plane sizes, and observation plane distances from the transmitting antenna array was carried out. Compared to previous works in [12–15], the proposed designs achieved broader bandwidth, meeting the 5G-mid-band requirement as well as it is much compact with simple design. The previous works did not carry out mode purity analysis, whereas a detailed mode purity analysis is carried out in this paper, which would assist the researchers and engineers in deciding the antenna size at receiving side to capture the incoming OAM waves from the transmitting side. This paper is organized as follows. The design of the antenna arrays is described in Section 2. Next, in the subsection of Section 2, the simulation results of the two designs are presented, such as phase difference and amplitude, as well as the fabrication process. The reflection coefficient ( $S_{11}$ ), bandwidth, phase distribution, current distribution, E-field vector, 2D radiation pattern, gain plot and mode purity are discussed in the subsequent section. Finally, conclusions are drawn in Section 4.

## 2 Antenna Design

In this section, the design of the antenna arrays to generate OAM waves for the 5G mid-band is presented. The antenna arrays consist of rectangular microstrip patch antennas, which are uniformly arranged in a circle and excited with a common input feeding. The overall design specification is tabulated in [Tab. 1](#).

**Table 1:** Design specifications of this work

Parameters	Requirements
Operating frequency	3.5 GHz
Bandwidth	Minimum 100 MHz
Reflection coefficient	$> -10$ dB
Input impedance	$50 \Omega$
OAM confirmation	Null in beam center, helical/spiral phase front and donut shape intensity if mode $\neq 0$

### 2.1 Individual Patch Design

The UCAs comprise identical microstrip patch antennas, which are uniformly placed in a circle on an FR-4 substrate with a thickness of 1.6 mm and a dielectric constant of 4.3. Microstrip patch antennas mainly comprise a radiating layer, substrate, and ground plane [16,17]. The substrate itself is located on a ground plane. The microstrip patch antenna design is selected for this experiment due to its low profile, low cost, easy fabrication, and lightweight [18]. The dimension of the single antenna element is calculated based on equations 1-5 [19]. Once the calculated dimensions were obtained, the following procedure was to design the antenna using CST Studio Suite 2019 software. However, the calculated antenna design did not operate at the desired frequency of 3.5 GHz. In addition, the reflection coefficient (S11) of the calculated design at 3.5 GHz was  $-7.10$  dB which showed a poor impedance matching, and sufficient power could not be transferred to the patch. Consequently, the antenna dimensions were optimized, and the inset feed technique was applied. Inset Feed causes high impedance matching so that maximum power from the generator side reaches near the center of the patch [20]. The dimensions of the optimized patch antennas are shown in Fig. 2a, which are chosen to meet the requirements in Tab. 1. The simulated parameter obtained using CST 2019 studio is shown in Fig. 2b. It can be seen that the patch antenna has a resonance at the desired frequency of 3.5 GHz. Reflection coefficient (S11) value of  $-42.76$  dB at the operating frequency indicated sufficient power is transferred to the patch antenna from the source.

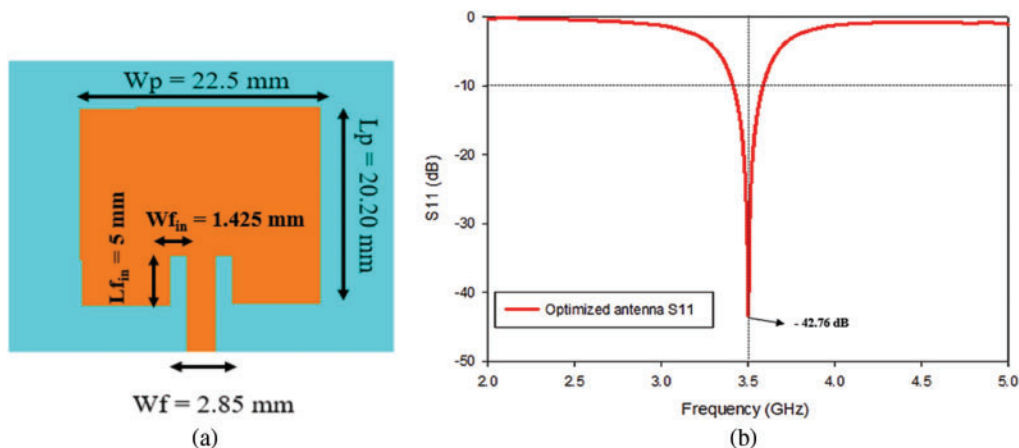


**Figure 2:** Individual patch antenna (a) Optimized dimension (b) S11 value at 3.5 GHz for the optimized antenna

## 2.2 UCA Design

Two uniform circular arrays (UCA) are designed, one with four elements (UCA-1) and the other with eight elements (UCA-2). For an  $N$ -element UCA, an OAM wave of topological charge  $l$  can be generated by exciting the elements with power of equal amplitude, but of a phase difference of  $\Delta\phi = \frac{2\pi l}{N}$ , between adjacent elements [21]. Therefore, to generate OAM mode  $+1/-1$ , for UCA-1, the phase difference has to be  $90^\circ$ , and for UCA-2 the phase difference has to be  $45^\circ$ . The dimensions for UCA-1 and UCA-2 are summarized in Tab. 2.

**Table 2:** UCA-1 and UCA-2 dimensions

Antenna design	Array dimension ( $W_g \times L_g$ )	Array radius
UCA-1	185 mm $\times$ 160 mm	73 mm
UCA-2	185 mm $\times$ 210 mm	84 mm

## 2.3 Feed Network Design

For each of the UCAs, their elements are excited by a single source. Equal power distribution to the elements is achieved using a feed network with T-junction dividers. The desired phase difference between adjacent elements is achieved by manipulating the feed line's lengths and the structure's symmetry. The feed network of UCA-1 is shown in Fig. 3a with patches and Fig. 3b without patches, consisting of five ports. Port 1 is the input port, whereas Port 2, Port 3, Port 4, and Port 5 are the output ports used to excite Patch 1, Patch 2, Patch 3, and Patch 4, respectively. The feed network design to achieve the desired phase difference between adjacent elements proceeds as follows. The feed network is divided into the lower part (Port 2 and Port 3) and the upper part (Port 4 and Port 5), as illustrated in Fig. 3b. First, the feed network for the lower part is designed. Power of equal amplitude to Port 2 and Port 3 is achieved using a T-junction divider. A phase difference between the power at Port 2 and Port 3 is achieved by optimizing the lengths of the feedlines. The upper part of the feed network is then constructed, identical to the lower part but rotated, as shown in Fig. 3b. The patches are then attached to their respective ports, with the patches in the lower part-oriented upside down concerning those in the upper part. That means, being fed with the power of the same phase, Patch 1 and Patch 3 have a phase difference of  $180^\circ$ . Therefore, the requirement for the  $90^\circ$  phase shift increment from Patch 1 to Patch 4 is satisfied. The same technique was applied for UCA-2 feeding network and the overall feeding network of UCA-2 is shown in Figs. 3c and 3d.

For UCA-1, the overall phase difference for patch 1 (port 2), patch 2 (port 3), patch 3 (port 4), and patch 4 (port 5) were  $4.53^\circ$ ,  $95.76^\circ$ ,  $6.63^\circ$ , and  $96.9^\circ$  as shown in Fig. 4a. The additional  $180^\circ$  phase shift due to the mirror image of the feeding network gives port four an overall phase shift of  $184.53^\circ$  and port five a phase shift of  $276.9^\circ$ . As a consequence, the incremental phase shift for UCA-1 is  $4.53^\circ$ ,  $95.76^\circ$ ,  $184.53^\circ$ , and  $276.9^\circ$ . The phase difference between patch one and patch 2 is  $91.23^\circ$ , patch two and patch 3 is  $88.77^\circ$ , patch three and patch 4 are  $92.37^\circ$ , and patch four and patch 1 are  $87.63^\circ$ . Based on the calculated value, the phase difference among the adjacent elements should be  $90^\circ$ , and from the simulation results, it has been observed that the obtained values are close to  $90^\circ$ . Some differences between calculated and simulated values are due to the misalignment of the output ports. Moreover, the amplitude was almost similar for all the four radiating elements, as shown in Fig. 4b. The amplitude for patches 1 (port 2), 2 (port 3), 3 (port 4), and 4 (port 5), were  $-8.91$  dB,  $-9.76$  dB,  $-8.84$  dB and  $-9.6$  dB.

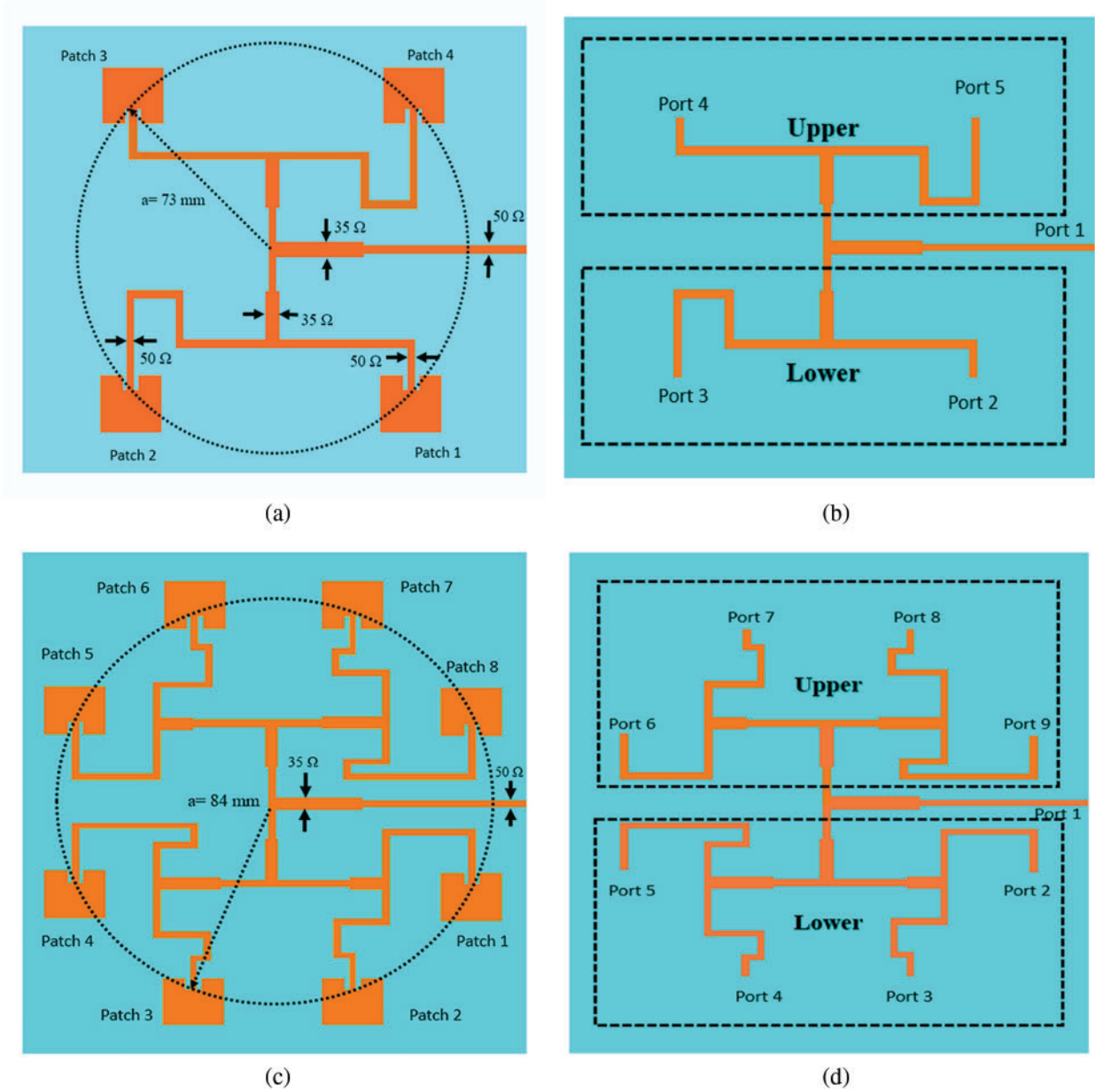


**Figure 3:** Simulated circular array antenna (a) UCA-1 radiating patch configuration (b) The feeding network of UCA-1 (c) UCA-2 radiating patch configuration (d) The feeding network of UCA-2

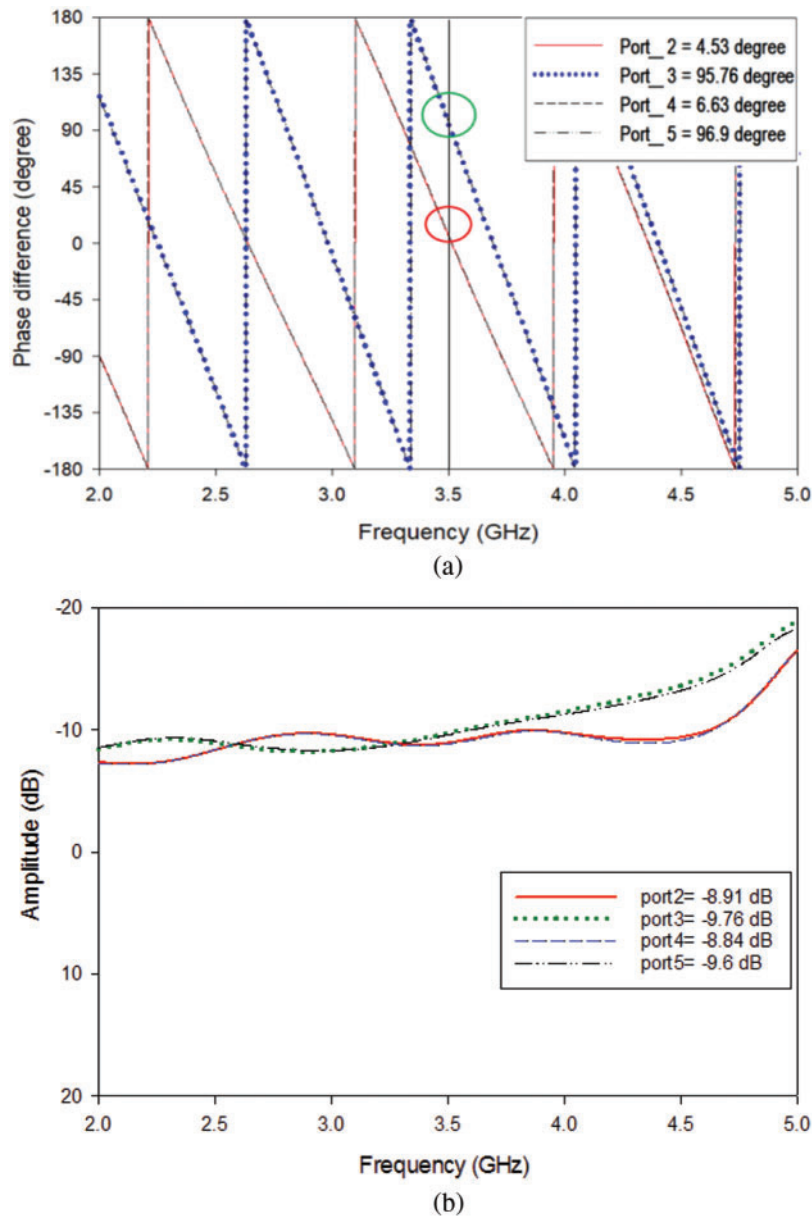


**Figure 4:** The Simulated results of UCA-1 (a) Phase shift among the elements (b) Amplitude of radiating patches

For UCA-2, the phase difference for patch 1 (port 2), patch 2 (port 3), patch 3 (port 4), patch 4 (port 5), patch 5 (port 6), patch 6 (port 7), patch 7 (port 8) and patch 8 (port 9) were  $8.04^\circ$ ,  $51.22^\circ$ ,  $97^\circ$ ,  $142.8^\circ$ ,  $9.5^\circ$ ,  $49.22^\circ$ ,  $90.4^\circ$  and  $134.7^\circ$  respectively as depicted in Fig. 5a. Due to the mirror image of the feeding network, an additional  $180^\circ$  phase shift is added from patch 5 to patch 8. Hence, the incremental phase shift for UCA-2 is  $8.04^\circ$  (patch 1),  $51.22^\circ$  (patch 2),  $97^\circ$  (patch 3),  $142.8^\circ$  (patch 4),  $189.5^\circ$  (patch 5),  $229.22^\circ$  (patch 6),  $270.4^\circ$  (patch 7) and  $314.7^\circ$  (patch 8). According to the calculated value, the phase difference between the adjacent elements for UCA-2 should be  $45^\circ$ , and it is observed from the simulation results that the obtained values are close to  $45^\circ$ . Furthermore, the amplitude at

port 2 to port 9 were  $-12.75$  dB,  $-12.30$  dB,  $-12.75$  dB,  $-11.53$  dB,  $-14.27$  dB,  $-14.29$  dB,  $-11.73$  dB and  $-13.64$  dB as shown in Fig. 5b.

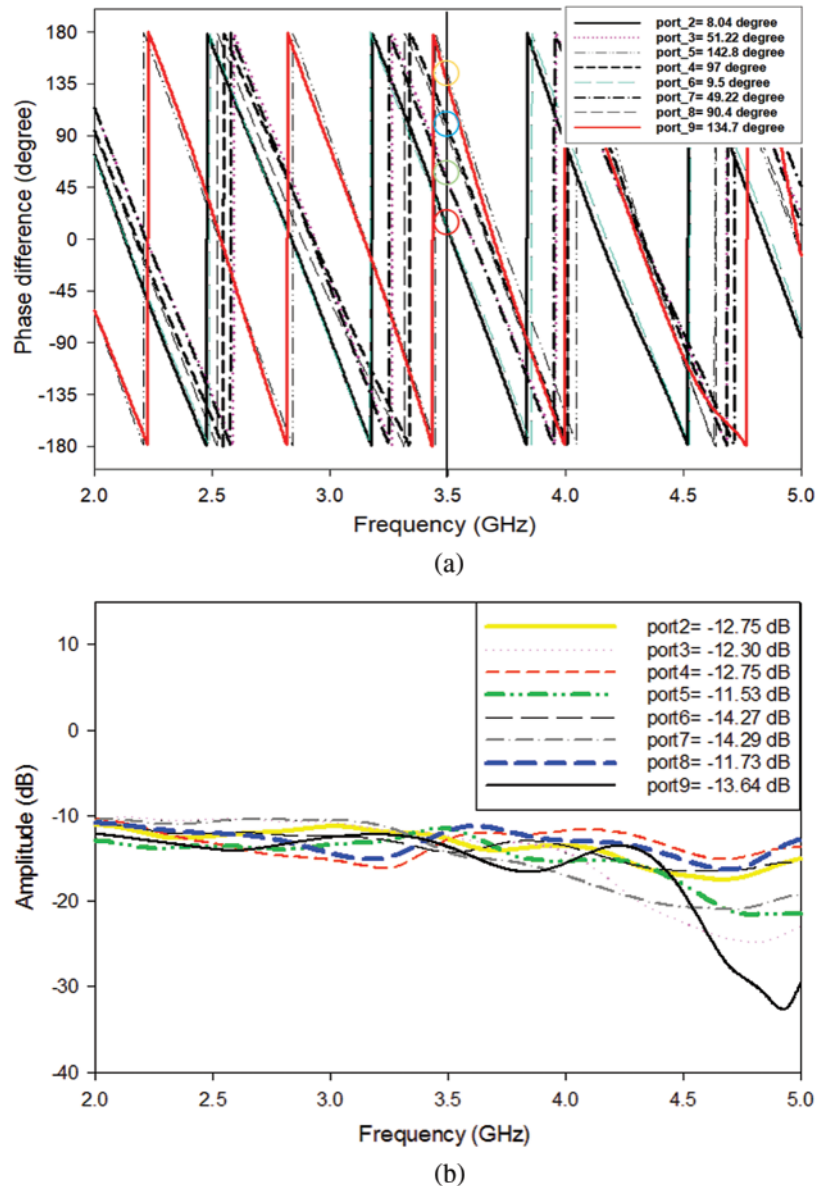


**Figure 5:** The simulated results of UCA-2 (a) Phase shift among the elements (b) Amplitude of radiating patches

Once the simulation result was obtained, the next task was to fabricate the prototypes, as shown in Figs. 6a and 6b. Moreover,  $50 \Omega$  SMA was connected at the standard input port to excite the radiating elements, as illustrated in Fig. 6c.

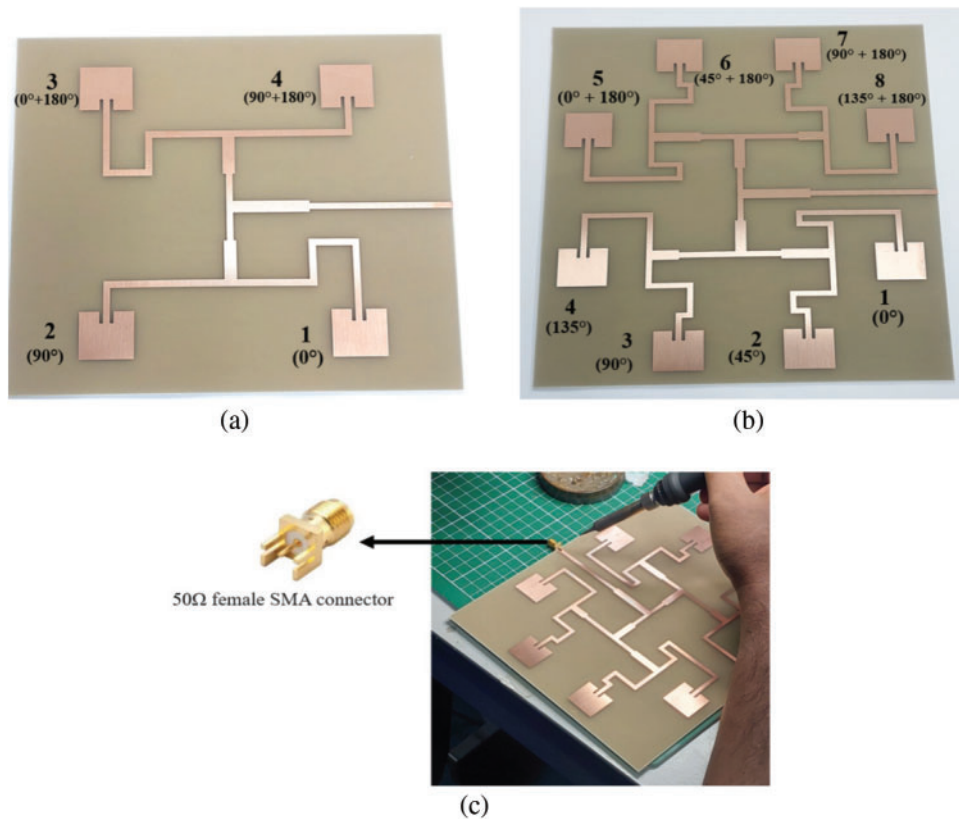


**Figure 6:** Prototype of the proposed designs (a) UCA-1 (b) UCA-2 (c) Soldering 50  $\Omega$  SMA connector

### 3 Experimental Setup, Results and Discussion

In this section, the results obtained from the simulation and experiment are discussed. Moreover, discussions regarding simulated and measured S11 values as well as bandwidth are summarized in this section. The simulated and measured 2D radiation pattern results prove that the proposed designs generated OAM mode 1 at the desired frequency band, and both the designs are compared with each other. Furthermore, the simulated gain obtained by UCA-1 and UCA-2 is also summarized in this section. Lastly, a detailed analysis of OAM mode purity was carried out based on the simulated designs where factors such as the number of antenna elements, observation plane radius, and distance from the transmitting antenna were taken into consideration to find out how it influences OAM mode purity.

#### 3.1 Phase and Intensity Distribution

To verify that the designed UCAs would generate OAM wave with mode 1, we first simulated the phase distributions of the radiation produced by the UCAs, on a transverse observation plane with a radius of 75 mm, located 600 mm away from the UCAs. Figs. 7a and 7b illustrated the simulated phase distributions of the radiation generated by the UCAs from 0° to 360°. From Figs. 7a and 7b, it is evident that both UCAs exhibit a spiral phase distribution with a continuous phase change around the centre, which is a characteristic feature of OAM wave. In addition, it can be observed from Fig. 7c that there is a donut structure at the centre (black dot inside the blue circle shape) of the beam, which depicts the intensity of the generated OAM mode. As reported in [22,23] that OAM vortex beams with

mode ( $l \neq 0$ ) have a donut shape structure, and this donut shape structure enlarges in size as the value of OAM modes ( $l$ ) increases. Therefore, both spiral wavefront and donut shape intensity is seen from the simulated results, which confirms the generation of OAM mode 1 using the proposed designs.

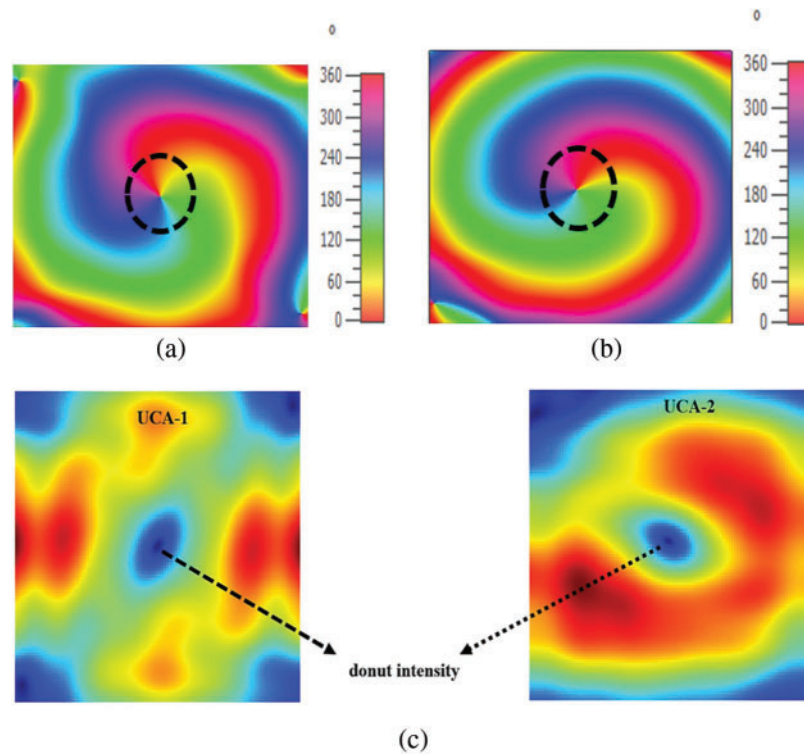
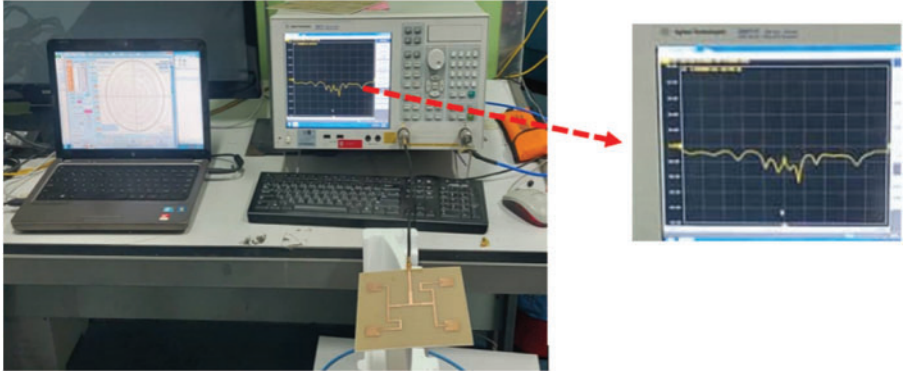


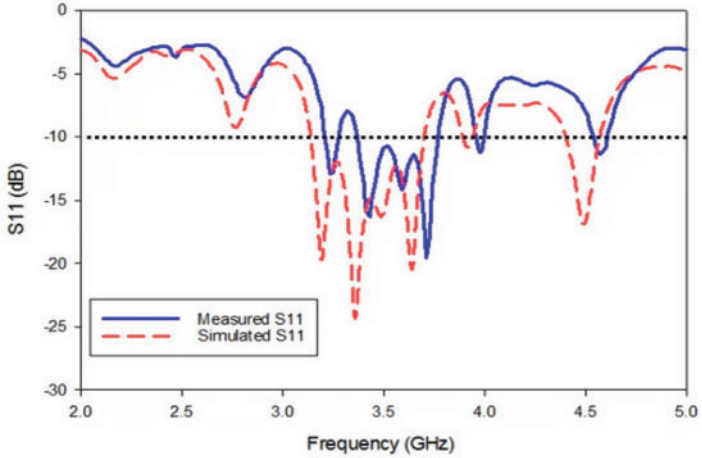
**Figure 7:** Simulated phase distribution of the radiation generated by (a) UCA-1 (b) UCA-2 (c) Simulated intensity of OAM mode 1

### 3.2 Reflection Coefficients and Bandwidth of the Proposed Designs

The measurement setup to measure the reflection coefficient ( $S_{11}$ ) and bandwidth of UCA-1 and UCA-2 are shown in Figs. 8a and 9a, respectively. The instrument used was Vector Network Analyzer (VNA) E5071C by Agilent Technologies. Fig. 8b shows the simulated and measured for UCA-1. It has been observed that the simulated  $S_{11}$  value was  $-15.92$  dB with a bandwidth value of 560.40 MHz for UCA-1. Nevertheless, during actual measurement, the obtained  $S_{11}$  value was  $-10.80$  dB with a bandwidth value of 420 MHz. For UCA-2, the simulated and measured results were very close. As shown in Fig. 9b, the simulated  $S_{11}$  value was  $-22.07$  dB with a bandwidth value of 547.4 MHz, while the measured  $S_{11}$  value was  $-22$  dB with a bandwidth value of 551.4 MHz. For UCA-2, the simulated and measured results matched very well compared to UCA-1. The simulated and measured results mismatch is attributed to fabrication error and measurement device uncertainty due to unequal lengths of coaxial lines and cables twisting. Nevertheless, both the designs have obtained an accepted  $S_{11}$  value and minimum 100 MHz bandwidth as per as the requirement of 5G mid-band deployment. It can observe that, for the same OAM mode 1, UCA-2 performed much better in terms of  $S_{11}$  value and bandwidth than UCA-1.

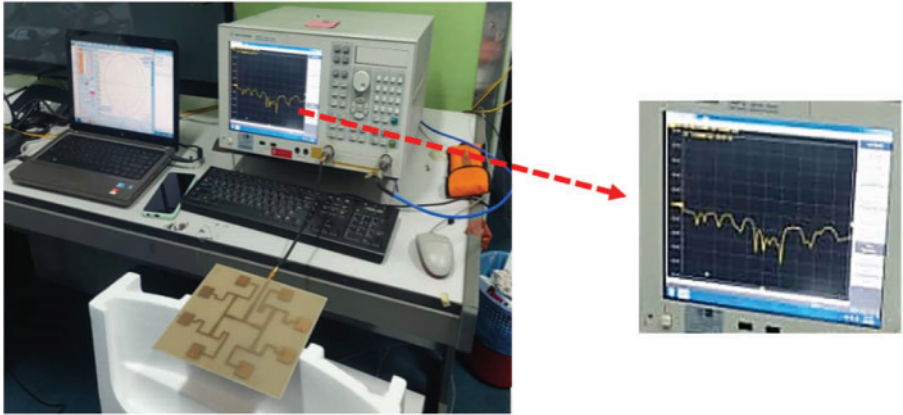


(a)



(b)

**Figure 8:** S11 and bandwidth measurement (a) UCA-1 measurement setup (b) Simulated and measured results of UCA-1



(a)

**Figure 9:** (Continued)

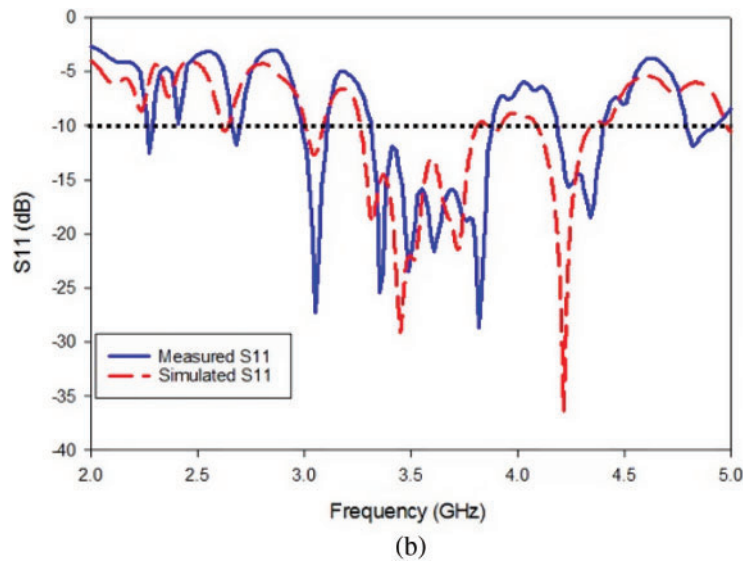


**Figure 9:** S11 and bandwidth measurement setup (a) UCA-2 setup (b) Simulated and measured results of UCA-2

### 3.3 Radiation Pattern

The experimental setup to measure the 2D radiation patterns in the E-plane of the UCAs is shown in Fig. 10a. The proposed designs acted as the transmitting antenna while the horn antenna at the other end acted as the receiving antenna, as shown in Figs. 10b and 10c. The entire setup was done inside the Anechoic chamber of Advanced Communication Engineering (ACE), Universiti Malaysia Perlis, Malaysia. The radiation pattern setup for UCA-1 and UCA-2 are shown in Figs. 10b and 10c, respectively.

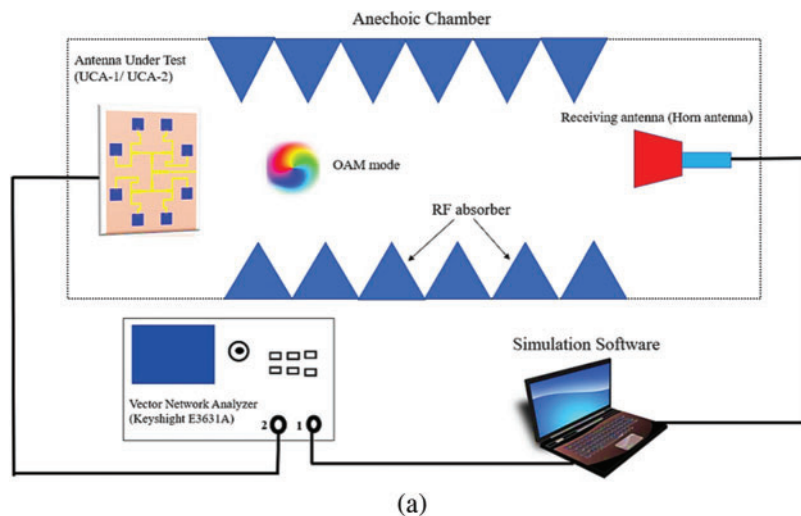


**Figure 10:** (Continued)

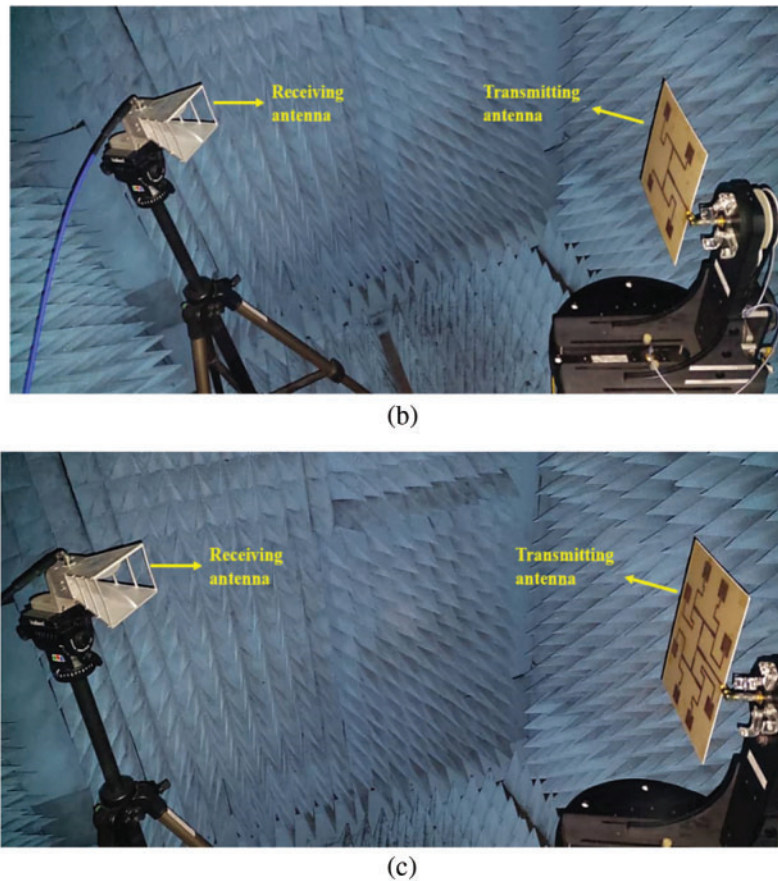


**Figure 10:** 2D radiation pattern measurement (a) Overall graphical presentation of the measurement setup (b) UCA-1 setup (c) UCA-2 setup

The simulated and measured normalized 2D polar radiation pattern at  $\phi = 0$  (E-plane or  $xz$  plane) is shown in Fig. 11. As shown in Fig. 11, the simulation and measurement results of the radiation pattern are in good agreement for UCA-1 and UCA-2. An intensity null in the center of the radiation pattern, characteristic of OAM waves [24], is apparent in the plot. For UCA-2, the intensity null in the centre is more pronounced, suggesting that a more significant number of elements produces a purer OAM mode. However, there are some differences between the simulation and measurement results due to variations in fabrication and the presence of the Antenna Under Test (AUT) stand. Moreover, it can be observed that the measured beamwidth is narrower than the simulated beamwidth for both UCA-1 and UCA-2. In addition, compared to UCA-1, there are more sidelobes present in UCA-2, as shown in Fig. 11b for the same OAM mode 1. It is because there are eight radiating elements in UCA-2 which caused the array to be more extensive in size, while there are four radiating elements in UCA-1. When the array size increases, the beamwidth becomes more directive; however, the sidelobes increase. Another significant observation can be made from Fig. 11b. When the antenna number radiating element increases and array size enlarges, the sidelobes become closer to the main lobe. If the sidelobes become close to the main lobe, it causes a significant energy loss. Therefore, several radiating elements and overall array size must be considered while generating OAM waves using circular array antennas. In addition, the simulated gain and directivity of UCA-1 were 3.245 dBi

and 9.265 dBi, respectively. For UCA-2, the gain obtained was 2.346 dBi, and directivity was 9.161 dBi. The simulated gain for the proposed designs is illustrated in Fig. 12. The gain is lower for UCA-2 because of the side lobes [25] since the array radius for UCA-2 is 84 mm while the radius is 73 mm for UCA-1. This increased array radius size will narrow the main lobe beam width and increase the side lobe radiation [26].

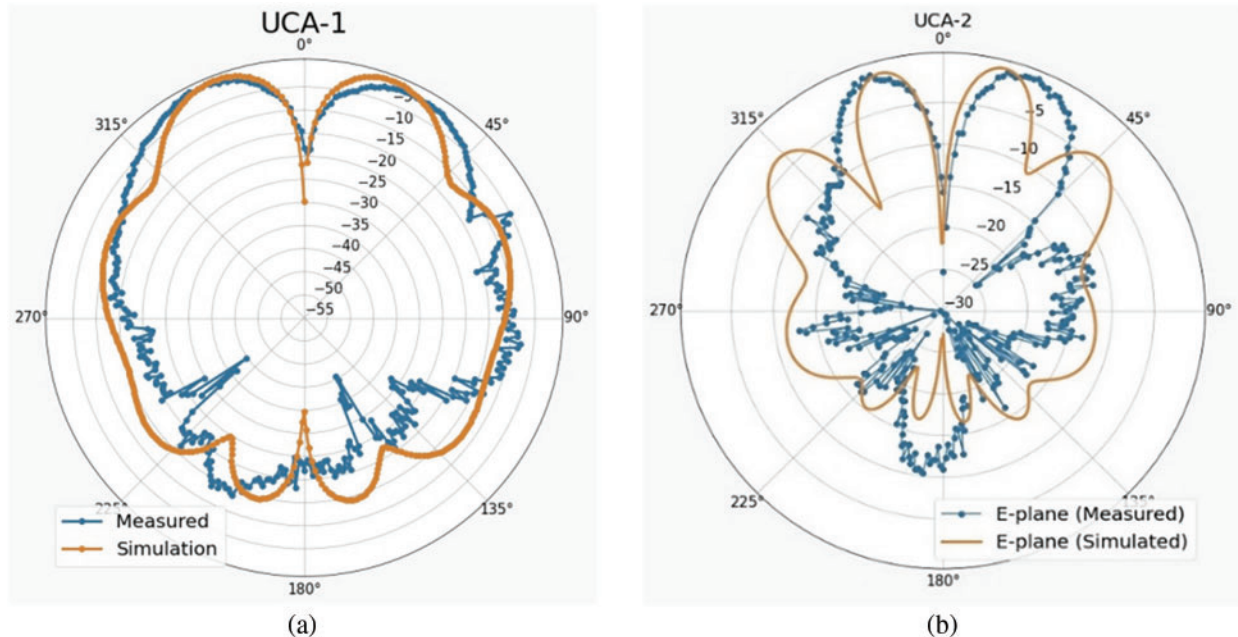


**Figure 11:** Simulated and measured 2D radiation pattern in E-plane for (a) UCA-1 (b) UCA-2

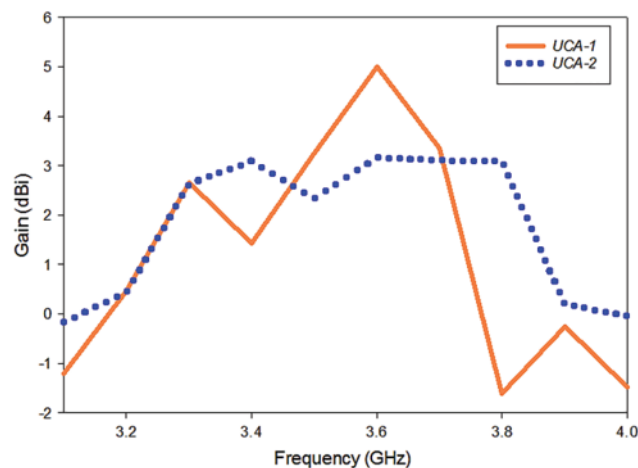


**Figure 12:** Simulated gain for UCA-1 and UCA-2

### 3.4 Current Distribution, Vector and Magnitude of Electric Field

The simulated current distribution of UCA-1 and UCA-2 designs at 3.5 GHz is shown in Fig. 13. The charges must accelerate and decelerate to create a time-varying current to create radiation.

Therefore, on a patch, how the charges are accumulated and where the charges are accumulated are explained by the current distribution in Fig. 13. It can be observed from Fig. 13a that the current distribution for patches 1 and 3 takes place together along the edges, while there is no distribution for patches 2 and 4. Furthermore, it can be seen from Fig. 13b that the current distribution is along the edges of patches 2 and 4, while there is the current distribution from the edges of patches 1 and 3. It is due to the difference in phase and feedline length. Similar behaviour can be observed in Figs. 13c and 13d. The current distribution illustrates that the wave is launched from the transmission line to the patch. Furthermore lastly, the wave is radiated from the edges of the patch. The current distribution at the edge of the patch element has also been observed in [27]. As modal currents are focussed on the edges, the length of the edges significantly impacts the resonance frequency of the characteristic modes.

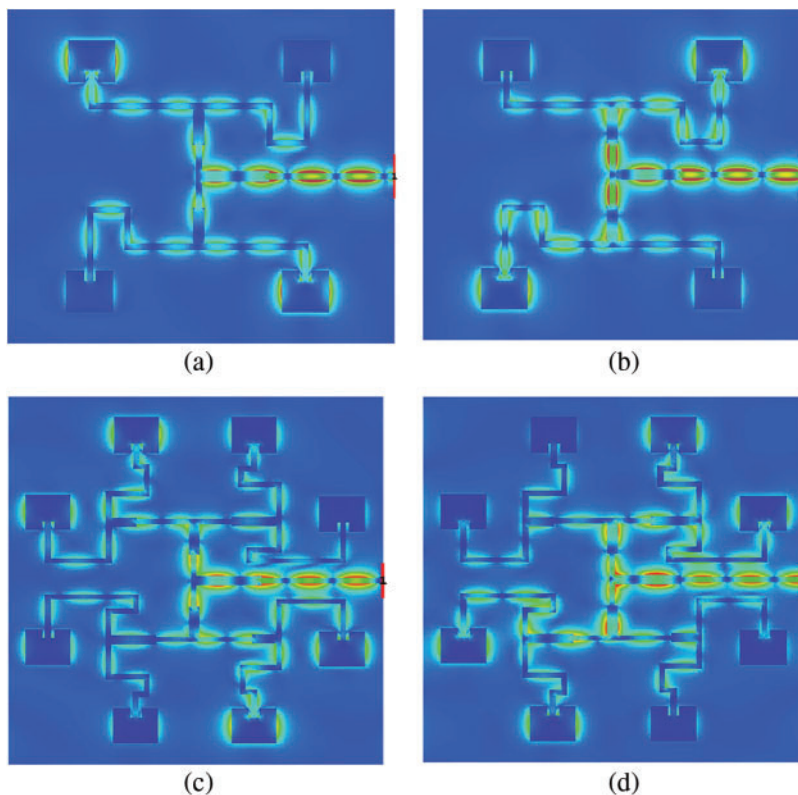


**Figure 13:** Surface current distribution at 3.5 GHz (a) Patch 1 and 3 of UCA-1 (b) Patch 2 and 4 of UCA-1 (c) Patch 1, 2, 5 and 6 of UCA-2 (d) Patch 3, 4, 7 and 8 of UCA-2

The vector and magnitude of the electric field at 3.5 GHz of UCA-1 and UCA-2 at three different phases, namely, phases 0, 180, and 360, are shown in Tab. 3. The concerned area, where the vector and magnitude of electric field (V/m) are plotted, is placed above the proposed circular array antennas and perpendicular to the  $z$ -axis. The overall size of the concerned area is 150 mm  $\times$  150 mm, and the distance between the antenna array and the concerned area is 600 mm. A helical or spiral shape electric field distribution can be observed from the results tabulated in Tab. 3. The spiral shape of the electric field for UCA-2 is more evident than for UCA-1. Hence, UCA-2 generated a purer OAM mode than UCA-1.

**Table 3:** The vector and magnitude of the E-field of the proposed designs

Design	Phase = 0	Phase = 180	Phase = 360
UCA-1			
UCA-2			

### 3.5 Mode Purity Analysis

To quantitatively evaluate the mode purity of the OAM modes generated by the UCAs, we performed an analysis using a Fourier transform [28]. The mode purity of an OAM wave is defined as the ratio of the power in the dominant mode to the total power of the wave. The power in mode is given by Eqs. (1) and (2) below.

$$\alpha(\phi) = \sum_c^r A_l \exp(il\phi) \tag{1}$$

$$A_l = \frac{1}{2\pi} \int_{-\pi}^{\pi} \alpha(\phi) \exp(-il\phi) d\phi \tag{2}$$

where  $\alpha(\phi)$  is the phase distribution of the generated OAM wave to be analyzed. In this work, the mode purity analysis is performed using the phase distribution obtained from CST simulation instead of measurement. The analysis is carried out for UCA-1 and UCA-2 for different observation plane radius ( $r$ ) and for different observation plane distances ( $z$ ) from the UCAs, as shown in Fig. 14.

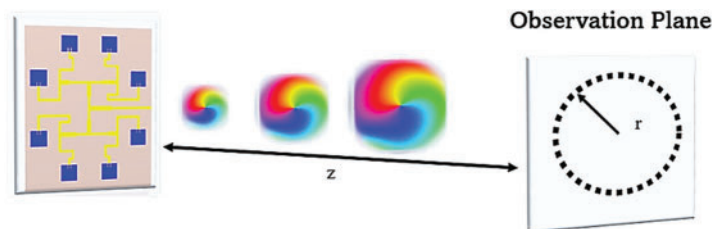


**Figure 14:** Simulation setup of the mode purity analysis

From [Tab. 4](#), it can be observed that UCA-2 generated OAM mode 1 with higher purity compared to UCA-1. This observation is consistent with the simulated phase distribution in [Fig. 7](#) and the measured radiation pattern in [Fig. 11](#). Therefore, it can be concluded that the greater the number of elements, the purer the generated OAM mode is. For both UCAs, the mode purity increases with the observation plane radii for a fixed observation plane distance. Similarly, for a fixed observation plane radius, the mode purity increases with the observation plane distance from the UCAs. For this paper, the mode purity of UCA-1 was 56.14%, while the mode purity of UCA-2 was 64.78%, as demonstrated in [Figs. 15a](#) and [15b](#), respectively. A 180-degree phased ambiguity produced the spurious modes [29], and a more negligible phase difference among adjacent radiating elements can minimize the phase ambiguity impact. This is why, based on the achieved results, more radiating elements are preferred to produce OAM mode with higher purity using the uniform circular array (UCA) method. The extensive study on the OAM mode purity can conclude that higher radiating elements are required to generate higher purity of OAM mode; however, having more radiating elements can make the design complex and unrealistic. Hence, a proper design and approach are required to generate high purity OAM mode.

**Table 4:** Mode purity analysis on UCA-1 and UCA-2

z	r						Remarks
	r = 10 mm		r = 45 mm		r = 75 mm		
	UCA-1	UCA-2	UCA-1	UCA-2	UCA-1	UCA-2	
z = 100 mm	43.11%	48.06%	43.62%	54.72%	44.61%	55.4%	UCA-2 is better in purity.
z = 200 mm	60.55%	58.35%	43.62%	62.87%	56.97%	57.18%	UCA-2 is better in purity.
z = 300 mm	64.48%	64.92%	53.48%	61.39%	43.05%	64.32%	UCA-2 is better in purity.
z = 400 mm	58.35%	66.72%	59.13%	64.83%	48.59%	62.68%	UCA-2 is better in purity.
z = 500 mm	48.86%	61.16%	60.63%	68.28%	55.83%	65.15%	UCA-2 is better in purity.
z = 600 mm	47.97%	53.62%	60.63%	66.56%	56.14%	64.78%	UCA-2 is better in purity.

[Tab. 5](#) compared the performance of the proposed designs with several other published works. It is evident that the designs of this paper are smaller in size and achieved wider bandwidth compared to other designs. As a matter of fact, UCA-2 is much better in terms of OAM purity and bandwidth than UCA-1.

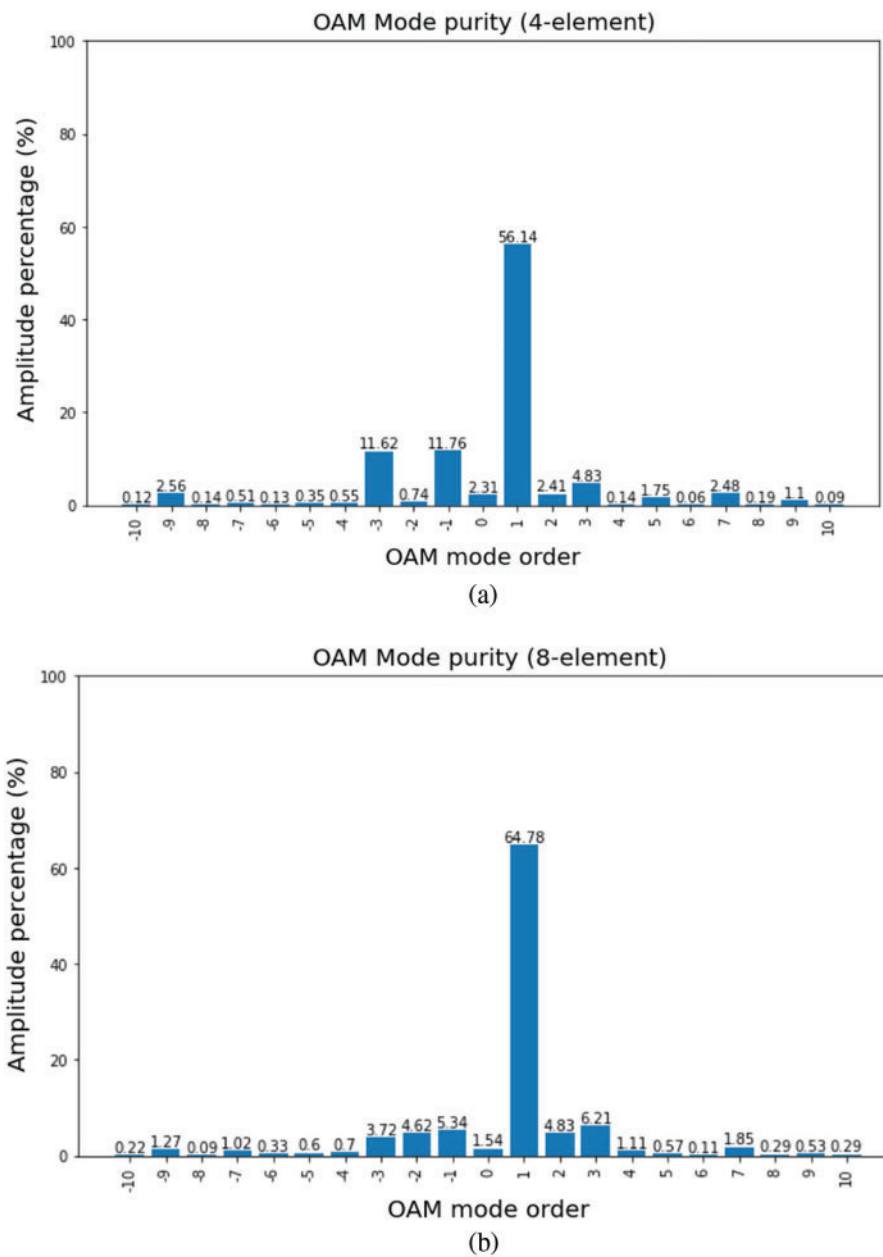


**Figure 15:** Simulation results of generated OAM mode purity (a) UCA-1 (b) UCA-2

**Table 5:** Comparison with previous works

References	Antenna dimension	5G mid-band frequency	Bandwidth	Mode purity percentage	Number of OAM modes
[12]	N/A	No	<300 MHz	N/A	1
[13]	N/A	No	<100 MHz	N/A	1

(Continued)

**Table 5:** Continued

References	Antenna dimension	5G mid-band frequency	Bandwidth	Mode purity percentage	Number of OAM modes
[14]	300 mm × 300 mm	No	150 MHz	N/A	1
[15]	N/A	No	500 MHz	N/A	1
UCA-1 (This work)	185 mm × 160 mm	Yes	420 MHz	56.14%	1
UCA-2 (This work)	185 mm × 210 mm	Yes	551.4 MHz	64.78%	1

#### 4 Conclusion

Two FR-4-based rectangular microstrip patch antennas with inset fed technique and uniform circular array configuration are designed and compared to generate OAM mode 1 at 3.5 GHz for 5G mid-band. Moreover, a mirror image arrangement of the feeding network is adopted to make the overall design approach simple and less complex. In addition, a detailed analysis of the effect of the number of radiating patches, size of the observation plane, and the distance between the transmitting antenna and observation plane on generating OAM mode purity are carried out in this paper. In terms of mode purity, it can be concluded that a more significant number of antenna elements shall increase the purity of generated OAM mode. If the observation is more significant in size and far from the transmitting antenna, more OAM beams can be detected by the observation plane. To further validate the performance of the proposed designs, the 2D far-field radiation patterns are measured using a standard horn antenna, and the measured results coincide well with the simulated ones. The measured results show that the antenna arrays can cover the 3.5 GHz band of the 5G Radio-frequency (RF) spectrum. The electric field phase patterns confirm the generation of OAM beams. From this paper, UCA-2 generated an OAM mode of high purity and achieved wider bandwidth than UCA-1. UCA-2 generated OAM mode with the purity of 64.78% with a bandwidth of 551.4 MHz, while UCA-1 generated OAM mode with the purity of 56.14% and bandwidth achieved was 420 MHz. Future work can include the use of slot on the patch antenna to increase the bandwidth [30]. As future wireless communication system would enhance the data rate and more channel capacity [31] hence it could be interesting to explore the possibility of generating multiple OAM modes at a 5G mid-band with higher purity. After comparing with some previous publications, this approach is believed to be significant progress in generating a low profile, high performance in terms of bandwidth, and space-saving configuration to generate OAM waves at 5G mid-band frequency. Lastly, the mode purity analysis of this paper shall guide future researchers and engineers in selecting the receiver size of the OAM wave based wireless communication system.

**Funding Statement:** This work was supported by Ministry of Higher Education through the Fundamental Research Grant Scheme (FRGS) under a grant number of FRGS/1/2020/ICT09/UNIMAP/02/2.

**Conflicts of Interest:** The authors declare that they have no conflicts of interest to report regarding the present study.

#### References

- [1] K. G. Eze, M. N. O. Sadiku and S. M. Musa, "5G wireless technology: A primer," *International Journal of Scientific Engineering and Technology*, vol. 7, no. 7, pp. 62–64, 2018.
- [2] T. Cisco and A. Internet, "Cisco: 2020 CISO benchmark report," *Computer Fraud & Security*, vol. 2020, no. 3, pp. 4, 2020.

- [3] A. Osseiran, F. Boccardi, V. Braun, K. Kusume, P. Marsch *et al.*, “Scenarios for 5G mobile and wireless communications: The vision of the METIS project,” *IEEE Communications Magazine*, vol. 52, no. 5, pp. 26–35, 2014.
- [4] Y. Yan, G. Xie, M. P. J. Lavery, H. Huang, N. Ahmed *et al.*, “High-capacity millimetre-wave communications with orbital angular momentum multiplexing,” *Nature Communications*, vol. 5, no. 4876, pp. 1–9, 2014.
- [5] H. Su, X. Shen, G. Su, L. Li, J. Ding *et al.*, “Efficient generation of microwave plasmonic vortices via a single deep-subwavelength meta-particle,” *Laser and Photonics Reviews*, vol. 12, no. 9, pp. 1–6, 2018.
- [6] J. Wang, S. Li, C. Li, L. Zhu, C. Gui *et al.*, “Ultra-High 230-bit/s/Hz spectral efficiency using OFDM/O-QAM 64-QAM signals over pol-muxed 22 orbital angular momentum (OAM) modes,” in *Proc. Optical Fiber Communication Conf., OFC 2014*, San Francisco, CA, USA, pp. 14–16, 2014.
- [7] L. Allen, M. W. Beijersbergen, R. J. C. Spreeuw and J. P. Woerdman, “Orbital angular momentum of light and the transformation of Laguerre-Gaussian laser modes,” *Physica Review A*, vol. 45, no. 11, pp. 8185–8189, 1992.
- [8] L. Jing, Z. Wang, X. Lin, B. Zheng, S. Xu *et al.*, “Spiral field generation in smith-purcell radiation by helical metagratings,” *Research*, vol. 2019, no. 17, pp. 1–8, 2019.
- [9] J. Xu, Y. Guo, P. Yang, R. Zhang, X. Zhai *et al.*, “Recent progress on RF orbital angular momentum antennas,” *Journal of Electromagnetic Waves and Applications*, vol. 34, no. 3, pp. 275–300, 2020.
- [10] R. Chen, H. Zhou, M. Moretti, X. Wang and J. Li, “Orbital angular momentum waves: Generation, detection, and emerging applications,” *IEEE Communications Surveys and Tutorials*, vol. 22, no. 2, pp. 840–868, 2020.
- [11] W. Wei, K. Mahdjoubi, C. Brousseau and O. Emile, “Generation of OAM waves with circular phase shifter and array of patch antennas,” *Electronics Letters*, vol. 51, no. 6, pp. 442–443, 2015.
- [12] K. Bi, J. Xu, D. Yang, Y. Hao, X. Gao *et al.*, “Generation of orbital angular momentum beam with circular polarization ceramic antenna array,” *IEEE Photonics Journal*, vol. 11, no. 2, pp. 1–8, 2019.
- [13] L. Fang, H. Yao and R. M. Henderson, “OAM antenna arrays at E-band,” in *Proc. IEEE MTT-S Int. Microwave Symp. Digest*, Honolulu, HI, USA, pp. 658–661, 2017.
- [14] D. Liu, L. Gui, Z. Zhang, H. Chen, G. Song *et al.*, “Multiplexed OAM wave communication with Two-OAM-Mode antenna systems,” *IEEE Access*, vol. 7, no. c, pp. 4160–4166, 2019.
- [15] Q. Bai, A. Tennant, E. Cano and B. Allen, “An experimental phased array for OAM generation,” in *Proc. 2014 Loughbrgh. Antennas Propag. Conf. LAPC 2014*, Loughborough, UK, pp. 165–168, 2014.
- [16] L. Fang and R. M. Henderson, “Orbital angular momentum uniform circular antenna array design and optimization-based array factor,” in *Proc. 2019 Texas Symp. on Wireless and Microwave Circuits and Systems, WMCS*, Waco, TX, USA, pp. 1–4, 2019.
- [17] N. Ramli, S. K. Noor, T. Khalifa and N. H. Abd Rahman, “Design and performance analysis of different dielectric substrate based microstrip patch antenna for 5G applications,” *International Journal of Advanced Computer Science and Applications*, vol. 11, no. 8, pp. 77–83, 2020.
- [18] S. K. Noor, N. Ramli, N. M. Sahar and T. Khalifa, “Compact and wide bandwidth microstrip patch antenna for 5G millimeter wave technology: Design and analysis,” *Journal of Physics: Conference Series*, vol. 1878, no. 1, pp. 1–14, 2021.
- [19] K. W. S. Al Kharusi, N. Ramli, S. Khan, M. T. Ali and M. H. Abdul Halim, “Gain enhancement of rectangular microstrip patch antenna using air gap at 2.4 Ghz,” *International Journal of Nanoelectronics and Materials*, vol. 13, no. Special Issue ISSTE2019, pp. 211–224, 2020.
- [20] S. Shankar and H. Chaurasiya, “Inset feed microstrip patch antenna,” in *Proc. IEEE Int. Conf. on Computer Communication and Control, IC4 2015*, Indore, India, pp. 4–6, 2016.
- [21] Q. Bai, A. Tennant and B. Allen, “Experimental circular phased array for generating OAM radio beams,” *Electronics Letters*, vol. 50, no. 20, pp. 1414–1415, 2014.
- [22] S. Pachava, R. Dharmavarapu, A. Vijayakumar, S. Jayakumar, A. Manthalkar *et al.*, “Generation and decomposition of scalar and vector modes carrying orbital angular momentum: A review,” *Optical Engineering*, vol. 59, no. 4, pp. 1, 2019.

- [23] W. Lee, J. Y. Hong, M. S. Kang, B. S. Kim, K. S. Kim *et al.*, “Microwave orbital angular momentum mode generation and multiplexing using a waveguide butler matrix,” *ETRI Journal*, vol. 39, no. 3, pp. 336–344, 2017.
- [24] L. Fang, H. Yao and R. Henderson, “Design and performance of OAM modes generated using dipole arrays with different feeds,” in *Proc. IEEE Radio Wireless Symp., RWS*, Anaheim, CA, USA, vol. 2018, pp. 200–202, 2018.
- [25] M. K. Abdulhameed, M. S. M. Isa, I. M. Ibrahim, Z. Zakaria, M. K. Mohsen *et al.*, “Side lobe reduction in array antenna by using novel design of EBG,” *International Journal of Electrical and Computer Engineering*, vol. 10, no. 1, pp. 308–315, 2020.
- [26] Q. Bai, A. Tennant, B. Allen and M. U. Rehman, “Generation of orbital angular momentum (OAM) radio beams with phased patch array,” in *Proc. 2013 Loughborough Antennas and Propagation Conf., LAPC 2013*, Loughborough, UK, pp. 410–413, 2013.
- [27] C. Guo, X. Zhao, C. Zhu, P. Xu and Y. Zhang, “An OAM patch antenna design and its array for higher order OAM mode generation,” *IEEE Antennas Wireless Propagation Letters*, vol. 18, no. 5, pp. 816–820, 2019.
- [28] Y. Huang, X. Li, Q. Li, Z. Qi, H. Zhu *et al.*, “Generation of broadband high-purity dual-mode OAM beams using a four-feed patch antenna: Theory and implementation,” *Scientific Reports*, vol. 9, no. 1, pp. 1–10, 2019.
- [29] J. Sjöholm and K. Palmer, “Angular momentum of electromagnetic radiation. Fundamental physics applied to the radio domain for innovative studies of space and development of new concepts in wireless communications,” Diploma Thesis, Uppsala University, Sweden, 2009.
- [30] A. Gunjal and S. Kumar, “Gain enhancement in u-slotted broadband dual circularly polarized antenna for s-band radar applications,” in *2020 Int. Conf. Emerg. Smart Comput. Informatics, ESCI 2020*, Pune, India, vol. 4, pp. 124–128, 2020.
- [31] S. Kumar, A. S. Dixit, R. R. Malekar, H. D. Raut and L. K. Shevada, “Fifth generation antennas: A comprehensive review of design and performance enhancement techniques,” *IEEE Access*, vol. 8, pp. 163568–163593, 2020.